INSTITUTE OF PHYSICS PUBLISHING JOURNAL OF PHYSICS B: ATOMIC, MOLECULAR AND OPTICAL PHYSICS

J. Phys. B: At. Mol. Opt. Phys. **35** (2002) 1071–1084 PII: S0953-4075(02)30834-4

High-resolution vacuum–ultraviolet and ultraviolet photoionization spectroscopy of krypton

F Brandi, W Hogervorst and W Ubachs

Laser Centre, Department of Physics and Astronomy, Vrije Universiteit, De Boelelaan 1081, 1081 HV Amsterdam, The Netherlands

E-mail: brandi@nat.vu.nl

Received 15 November 2001
Published 13 February 2002
Online at stacks.iop.org/JPhysB/35/1071

Abstract

Accurate spectroscopy of krypton is performed on five transitions from the $(4p^6)$ $^1S_0$ ground state to the $5d[1/2]_1$, $6s[3/2]_1$, $5p[1/2]_0$, $5p[3/2]_2$ and $5p[5/2]_2$ excited states (jl-coupling notation) by means of 1VUV + 1UV and 2UV + 1UV resonance-enhanced photoionization. Isotope shifts of all six stable isotopes are determined, and a King plot analysis indicates a large field shift factor even for transitions in which no s electron is involved. Absolute frequency calibration is performed on three transitions, leading to a novel determination of the excited state energies of Kr with an accuracy of $\sim$0.0013 cm^{-1}. An accurate value for the ionization energy of ^{86}Kr, 112 914.516(14) cm^{-1}, is derived along with ionization energies for all even isotopes. The ac Stark effect on the two-photon transition to the $5p[1/2]_0$ excited state is investigated. For light intensities up to $\sim$260 MW cm^{-2} a linear shift of 0.75(48) Hz (W cm^{-2})$^{-1}$ is observed, while at higher intensities the line exhibits a sub-linear shift and an asymmetric broadening. Consequences of the results obtained for the $5p[1/2]_0$ state on resonance-enhanced narrow-band XUV/VUV generation are discussed.

1. Introduction

The level structure of the noble gas atoms displays manifolds of relatively closely packed electronically excited states separated by 10 eV or more from a single electronic ground state ($^1S_0$), without any fine or hyperfine structure. Optical spectroscopy, with classical methods, and laser spectroscopy, using the presence of one or more metastable levels, has allowed for precision experiments within the excited state manifolds. The ionization energies, with respect to the lowest lying excited states, were accurately determined through extrapolation of the Rydberg series; as examples we refer to laser spectroscopic work on the Rydberg series in krypton by Yoon and Glab [1] and in xenon by Knight and Wang [2]. Thus, a single accurate measurement of a transition frequency involving the $^1S_0$ ground state, yields

a value of the ionization energy of the atom. However, a complication is the production and calibration of narrow-band radiation at the wavelengths required, which all fall in the vacuum–ultraviolet (VUV) and extreme-ultraviolet (XUV) domains. Such studies have recently been performed on noble gas atoms using XUV/VUV laser sources based on nonlinear up-conversion of wavelength-tunable and narrow-band laser pulses in the visible range.

Eikema *et al* [3, 4] performed photoionization spectroscopy on the ($1\,^1$S–$2\,^1$P) transition in He at 58 nm, measuring the ^{3}He–^{4}He isotope shift (IS), the ac Stark shift and determining an accurate value of the transition frequency. From this value the ground state Lamb shift and an improved value of the ionization energy were obtained. A similar study on the two lowest resonance lines in neon near 74 nm was performed as well [5]. Velchev *et al* [6] measured IS values and the absolute frequency of the ($3p^6$–$3p^5 4s'[1/2]_1$) transition in Ar, also leading to an improved value for the ionization energy. Trickl *et al* [7] performed high-resolution photoionization spectroscopy of Kr in transitions from the ground state to several ns Rydberg levels. Transition frequencies, ISs, hyperfine splittings (HFSs) and lifetimes were measured, and accurate values for the excited state energies were deduced. Brandi *et al* [8] measured ISs, HFSs and transition frequencies of four transitions in Xe in the VUV range, from which isotope-dependent ionization energies were derived. King plot analysis [9] on the IS data revealed a large field shift factor, i.e. a big increase in the electron density at the nucleus during the transition; this phenomenon was ascribed to the removal of a p electron from the closed shell ground state configuration. In the case of xenon it was demonstrated by Plimmer *et al* [10] that the energy gap between the ground state and the manifold of electronically excited states could be bridged in two-photon excitation using cw-lasers; in the latter study no absolute calibration was performed of the transition frequency.

In this paper we report on 1VUV + 1UV and 2UV + 1UV photoionization spectroscopy on five transitions from the ground state of krypton. One-photon excitation is performed to the $5d[1/2]_1$ and $6s[3/2]_1$ excited states (jl-coupling notation) while $5p[1/2]_0$, $5p[3/2]_2$ and $5p[5/2]_2$ levels are investigated with two-photon excitation. Natural krypton gas is composed of six isotopes: ^{78}Kr (0.35%), ^{80}Kr (2.3%), ^{82}Kr (11.6%), ^{83}Kr (11.5%), ^{84}Kr (57.0%) and ^{86}Kr (17.3%). The odd ^{83}Kr is the only isotope with non-zero nuclear spin ($I = 9/2$), inducing a hyperfine structure on lines involving states with non-zero electronic angular momentum. ISs are measured for all transitions and a King plot analysis indicates the effect of a large field shift factor, as in the case of xenon. Accurate absolute energies are determined for the $5d[1/2]_1$, $6s[3/2]_1$ and $5p[1/2]_0$ excited states, leading to a determination of excited state energies of krypton at the 40 MHz accuracy level. This result, combined with data reported in the literature, enables us to estimate the ionization energies for all even isotopes.

Accurate spectroscopy of the $5p[1/2]_0$ excited state is of particular interest, since the two-photon ($4p^6$–$4p^5 5p[1/2]_0$) transition at 212.55 nm has been found to be very efficient for the production of XUV and VUV tunable radiation via resonance-enhanced third-harmonic generation and sum-difference frequency mixing in a Kr jet [11, 12]. Using this resonance-enhanced sum-frequency mixing scheme Balakrishnan *et al* [13] produced tunable XUV-radiation, which was applied in a determination of the dissociation energy of the hydrogen molecule. Hollenstein *et al* [14] built a tunable XUV laser source with a 0.008 cm^{-1} bandwidth based on this krypton resonance. Here we report on the ac Stark effect of the ($4p^6$–$4p^5 5p[1/2]_0$) transition. Results show a linear shift of the line at low light intensity and a sub-linear shift with asymmetric line profile at high intensity. The accurate analysis of the intensity effects on the transition frequency in this two-photon resonance bears relevance for the studies in which the tunable XUV/VUV output radiation is used in precision spectroscopy.

Table 1. Summary of experimental conditions; λ_{vis} and $\lambda_{VUV/UV}$ denote the wavelength of the primary cw visible and VUV or UV exciting radiation respectively (depending on the photoionization scheme used); in the last column the dyes used in the laser systems are reported.

Photoionization scheme	Excited state	λ_{vis} (nm)	$\lambda_{VUV/UV}$ (nm)	Dyes: Ring–PDA
1VUV + 1UV	$5d[1/2]_1$	578.0	96.3	Rh 6G–Rh B
	$6s[3/2]_1$	600.6	100.1	Rh 6G–Rh 101
2UV + 1UV	$5p[1/2]_0$	637.8	212.6	DCM–DCM
	$5p[3/2]_2$	644.4	214.8	DCM–DCM
	$5p[5/2]_2$	650.1	216.7	DCM–DCM

2. Experimental setup and procedure

2.1. 1VUV + 1UV photoionization spectroscopy

The experimental apparatus used to perform 1VUV + 1UV photoionization spectroscopy is discussed in previous papers [6, 8]; here only a brief description is given. The primary light source is a cw-tunable ring-dye-laser (Spectra Physics 380) running on Rhodamine 6G dye and pumped by a 5W frequency-doubled diode-pumped Nd:YVO_4 laser (Spectra Physics Millennia). The cw visible light is coupled into a single-mode polarization-maintaining fibre, whose output (typically 250 mW) seeds a pulsed-dye-amplifier (PDA). The PDA contains three amplifier stages pumped by the second harmonic of an injection-seeded Q-switched Nd:YAG laser (Quanta Ray, GCR-5), running at 10 Hz repetition rate, and delivering a maximum of 770 mJ/pulse at 532 nm. The 6 ns pulses from the PDA are frequency doubled in a KD*P crystal to generate UV radiation. The UV pulses (up to 30 mJ) are subsequently focused by a 25 cm focal length lens in a xenon gas jet where VUV coherent radiation is produced via third-harmonic generation. In a differentially pumped chamber the overlapping VUV and UV beams perpendicularly intersect a collimated Kr atomic beam. The ions produced by resonant 1VUV + 1UV photoionization are detected by an electron multiplier. A time-of-flight mass spectrometer is used to separate the signals for different isotopes, which are collected with boxcar integrators with gates set at the appropriate time windows. The recorded spectra are stored in a computer for further analysis. The wavelengths of the visible and VUV radiation needed to excite the $5d[1/2]_1$ and $6s[3/2]_1$ states are collected in table 1, where the dyes used in the laser system are also included.

Absolute frequencies in the VUV range are calibrated by performing metrology on the cw-seed input of the PDA, using a molecular iodine (I_2) saturation setup, and a temperature and pressure stabilized confocal Fabry–Pérot interferometer (FPI). The '*t*' hyperfine components of I_2 lines have been recently calibrated in the 571–655 nm wavelength range [15, 16] with 1 MHz accuracy (at 1σ), and give a very dense reference grid. The FPI transmission peaks are recorded during the scans, giving accurate frequency markers for the VUV radiation.

The VUV frequency scale is based on the metrology in the visible range after multiplication by a factor of 6. However, due to chirp effects in the amplification process, the centre frequency of the pulsed output of the PDA may undergo a small net shift with respect to the seeding cw light. This issue has been the subject of several studies [17–19]. The origin of chirp is a time-dependent gain in the amplification process, and its magnitude depends upon the dye used and the wavelength with respect to the maximum of the dye curve. In high-precision pulsed spectroscopy the chirp effect is the main source of systematic error, typically 0.003 cm^{-1}, and techniques have been developed to overcome it. Eyler *et al* [20] performed precision

2UV + 1UV photoionization spectroscopy of the ($EF \leftarrow X$) transition in H_2, reducing the chirp shift below the 10 MHz level using a particular mix of DCM and Rh 610 dyes. This technique, however, is applicable only to the very special case in which the transition to be investigated lies in a wavelength range where opposite chirp effects cancel the overall shift. Eikema *et al* [4] developed a technique to actively compensate the chirp effect by applying a phase modulation on the seeding light at the input of the PDA. They were able to significantly reduce the chirp shift, leaving a residual effect on the resonance position below the 10 MHz level. The PDA used in the present experiment is the same as the one used by Eikema *et al* [4], but without the anti-chirp compensation part.

2.2. 2UV + 1UV photoionization spectroscopy

2UV + 1UV photoionization spectroscopy is performed using the same experimental apparatus as described in the previous section. The wavelengths needed to perform two-photon excitations and the dyes used are also reported in table 1.

Tunable UV radiation around 215 nm is generated by tripling the visible output of the PDA, typically 60 mJ/pulse at full pump power. First type-I second harmonic generation is performed in a KD*P crystal, then sum-frequency mixing between fundamental and second harmonic beams takes place in a BBO crystal cut for type-I mixing. A zero-order half-wave plate, with axis set at 45° with respect to the vertical axes, is used to rotate by 90° the polarization of the visible radiation leaving the polarization of the second harmonic unchanged (in fact rotated by 180°). In this way type-I mixing takes place in the BBO crystal, and third-harmonic radiation is generated. The third-harmonic radiation is separated from the fundamental and the second harmonic using two dichroic mirrors, leaving 1 mJ/pulse useful energy in the UV.

In this experiment the UV beam, with or without focusing by a lens, intersects the Kr atomic beam in the interaction chamber and a two-photon resonant three-photon ionization process takes place. In the spectroscopic measurement involving two-photon excitation the UV-pulses are used in an unfocused geometry. Only for the measurements of the ac Stark effect is a 1 m focusing lens used to increase the power density in the interaction region.

3. Experimental results and discussion

The five investigated transitions are denoted by their excited state configurations, namely $5d[1/2]_1$, $6s[3/2]_1$, $5p[1/2]_0$, $5p[3/2]_2$ and $5p[5/2]_2$. Typical experimental results are presented in figure 1, where recorded spectra of the $5p[5/2]_2$ two-photon excitation and $5d[1/2]_1$ one-photon excitation are shown. Since three boxcars are used several scans are needed to cover the entire manifold of stable isotopes. The spectrum of the most abundant ^{84}Kr is recorded in every scan as a reference, and is used to put all the isotopic spectra on the same scale. The attainable signal-to-noise ratio allows for the observation of even the less abundant ^{78}Kr and ^{80}Kr isotopes. The etalon markers, and I_2 hyperfine line used for absolute frequency calibration of the $5d[1/2]_1$ transition, are also shown. The horizontal axis represents the actual transition frequency, i.e. VUV and 2UV frequency for one-photon and two-photon excitation respectively, while the origin is set at the second etalon fringe.

The recorded lines are fitted with a Gaussian profile and the resulting full-widths at half maximum (FWHM) are ∼400 and ∼350 MHz for 1VUV + 1UV and 2UV + 1UV photoionization experiments respectively. The line-widths predominantly reflect the band-width of the exciting radiation. The residual Doppler effect gives a minor contribution in the crossed beam configuration.

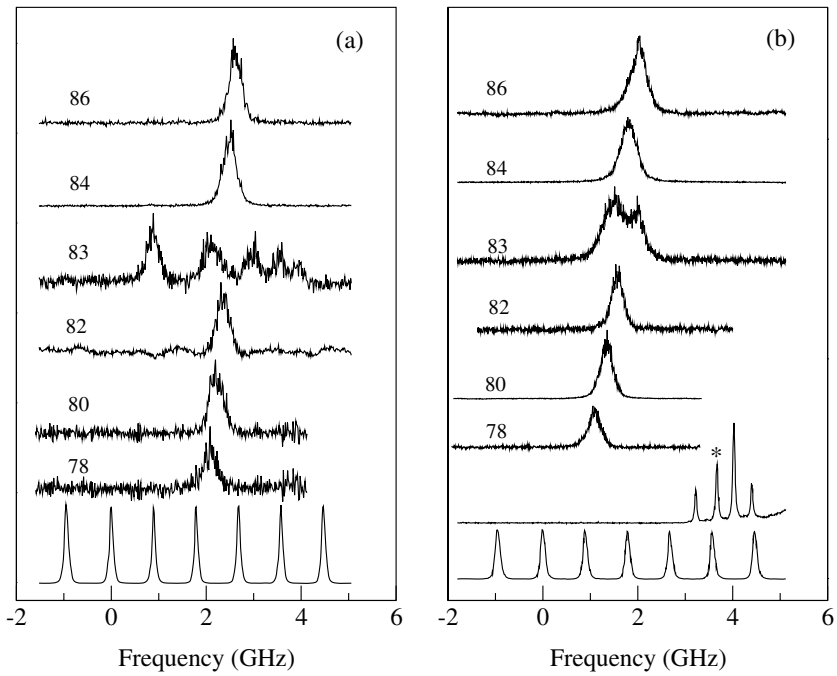

Figure 1. Photoionization spectra of Kr resonances for all stable isotopes: (*a*) two-photon excitation of the $5p[5/2]_2$ state with UV radiation at 216.7 nm in an unfocused geometry; the five hyperfine components of ^{83}Kr are resolved, with their F-value decreasing (from 13/2 to 5/2) with increasing frequency. (*b*) One-photon excitation of the $5d[1/2]_1$ state with VUV radiation at 96.3 nm; the three hyperfine components of ^{83}Kr are not resolved in this transition. In both graphs the etalon markers are scaled to the actual excitation energy; in (*b*) also the I_2-saturation spectrum of the P(11)16-1 line is shown, with the '*t*' hyperfine component denoted by (*). The spurious weak modulation present in the ^{82}Kr trace in (*a*) is noise introduced by the boxcar.

3.1. Isotope shift

The IS in an atomic transition i is defined as $\Delta_i^{A',A} = \nu_i^{A'} - \nu_i^A$, where ν_i^A denotes the transition frequency of the isotope with mass number A. For isotopes with nonzero nuclear spin I and atomic levels with nonzero angular momentum J, hyperfine splittings have to be considered. In the present experiment spectral lines of krypton are studied, pertaining to transitions from the ground state, which has $J = 0$. The hyperfine components directly reflect the excited state hyperfine structure, with states of different total angular momentum F. In this case the frequency shift between the line of an isotope of atomic mass number A' with zero nuclear spin, and the 'F' hyperfine component of an isotope with atomic mass number A and $I \neq 0$, is given by

$$\Delta_{i,F}^{A',A} = \nu_i^{A'} - \nu_i^A - \mathcal{A}\frac{C}{2} - \mathcal{B}\frac{\frac{3}{4}C(C+1) - I(I+1)J(J+1)}{2I(2I-1)J(2J-1)}, \tag{1}$$

where $\mathcal{A}$ and $\mathcal{B}$ are the magnetic dipole and electric quadrupole HFS constants of the excited state respectively, and $C = F(F+1) - I(I+1) - J(J+1)$. ν_i^A represents the transition frequency to the centre of gravity of the hyperfine structure.

The measured ISs relative to ^{84}Kr are presented in table 2 for all five transitions. The values reported are averaged over several scans; the uncertainty is the standard deviation. For the isotope ^{83}Kr, with nonzero nuclear spin ($I = 9/2$), the IS is evaluated relative to

Table 2. Summary of results on IS measurements, $\Delta_i^{84,A} = \nu_i^{84} - \nu_i^A$ (in MHz); reported uncertainties are 1σ; the claimed uncertainty in the values from [7, 23] is about 6 MHz.

Transition	86	83	82	80	78
$5d[1/2]_1$	−206(15)		226(10)	475(15)	709(15)
from [23]	−207				
$6s[3/2]_1$	−112(15)	91(14)	157(10)	284(15)	425(15)
from [7]	−132	21	116	230	384
$5p[1/2]_0$	−138(15)	88(17)	138(17)	311(16)	426(15)
from [23]	−141		150	306	445
$5p[3/2]_2$	−130(15)	83(16)	148(13)	295(14)	435(17)
from [23]	−132		147	294	438
$5p[5/2]_2$	−123(15)	95(15)	150(13)	303(15)	430(15)
from [23]	−132		141	291	429

the centre of gravity of the hyperfine structure. In the $5p[1/2]_0$ transition no HFS is present since $J = 0$, and $\Delta_i^{84,83}$ is measured directly. The individual hyperfine components are identified on the basis of the intensity rule [21], i.e. higher line intensity for larger F values. Due to the laser band-width the resolution is not always sufficient to resolve the hyperfine structure completely, and typically only the strongest component with the highest F value is fully resolved. For the $5d[1/2]_1$ transition not a single hyperfine component is resolved (see figure 1(*b*)); moreover, the signal from the ^{82}Kr isotope leaks into the mass-83 channel, obscuring the hyperfine components further. For example, the high-frequency tail of the $F = 11/2$ component in figure 1(*a*) corresponds to the ^{82}Kr line. For the $5p[3/2]_2$ and $6s[3/2]_1$ transitions $\Delta_i^{84,83}$ is evaluated via (1) using the measured $\Delta^{84,83}_{5p[3/2]_2,13/2} = 1083(14)$ MHz and $\Delta^{84,83}_{6s[3/2]_1,11/2} = 786(10)$ MHz, in combination with hyperfine constants reported in the literature [7, 22]. Only for the $5p[5/2]_2$ transition is the hyperfine structure sufficiently resolved to enable an evaluation of the hyperfine constants (see figure 1(*a*)). A least-squares fit applied to equation (1) using measured values for $\Delta^{84,83}_{5p[5/2]_2,F}$ ($F = 13/2, 9/2, 7/2, 5/2$), gives $\mathcal{A} = -155.6(1.2)$ MHz and $\mathcal{B} = -428(25)$ MHz, which are compatible with the values $\mathcal{A} = -156.49(8)$ MHz and $\mathcal{B} = -407.7(13)$ MHz reported in [22].

IS data reported in the literature are also presented in table 2 for comparison. The present results are compatible with the values reported by Kaufman [23], who systematically analysed IS data of krypton from interferometrically measured lines, and included some values of Trickl *et al* [7]. For the $6s[3/2]_1$ transition there is a discrepancy between our results and those of [7], especially for the ^{83}Kr isotope. To underline the consistency of our results it has to be noted that the latter data for the $6s[3/2]_1$ transition were not included in the analysis of Kaufman [23].

The IS of an atomic transition has two contributions, the mass shift, due to the finite mass of the nucleus, and the field shift, which arises from the nonzero volume of the nucleus [9]. The latter is predominant in heavy elements, while the former prevails in light elements. Formally the IS in a transition i can be expressed as [24]

$$\Delta_i^{A',A} = \Delta_{MS,i}^{A',A} + \Delta_{FS,i}^{A',A} = M_i \frac{A' - A}{AA'} + F_i \lambda^{A',A}, \tag{2}$$

where M_i and F_i are the so-called mass and field shift factors respectively, and the nuclear parameters $\lambda^{A',A}$ represent, to a good approximation, changes in mean-square nuclear charge radii between isotopes. The field shift factor is proportional to the change in the total electron density at the nucleus, and can be calculated using two different semi-empirical approaches based on the magnetic hyperfine structure and the Goudsmit–Fermi–Segrè formula [21], respectively. Evaluation of the mass shift factor requires complicated many-body atomic structure calculations; alternatively an estimate can be given by a combined analysis with muonic IS data.

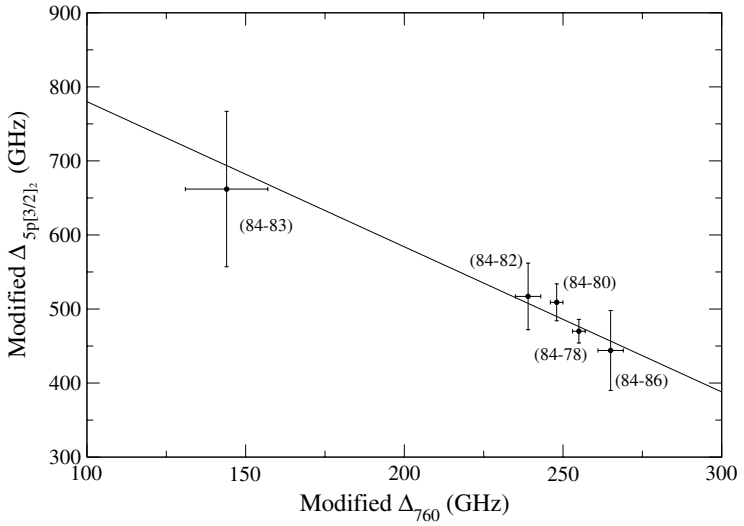

Figure 2. King plot of the IS in the $5p[5/2]_2$ transition, as measured in the present experiment, versus the IS in the $(5s[3/2]_2–5p[3/2]_2)$ transition at 760 nm [22]; the isotope pair is specified for each point and the straight line is the result of a weighted linear least-squares fit.

Table 3. Results of the IS analysis; the second and third columns contain the results from a weighted linear least-squares fit on the King plots; the values of the mass and field shift factors reported in the last two columns are obtained using $F_{760} = -0.605(30)$ GHz fm^{-2} and $M_{760} = 172(17)$ GHz from [25, 26].

Transition	(F_i/F_{760})	$[M_i - (F_i/F_{760})M_{760}]$ (GHz)	F_i (GHz fm^{-2})	M_i (GHz)
$6s[3/2]_1$	−2.04(83)	986(208)	1.23(50)	635(252)
$5p[1/2]_0$	−1.35(95)	821(254)	0.82(57)	589(302)
$5p[3/2]_2$	−1.06(95)	751(238)	0.64(57)	569(289)
$5p[5/2]_2$	−1.96(89)	976(225)	1.19(54)	639(272)

To extract physical information on the electronic structure of the atom from the present IS measurements, the so-called King plot analysis is performed [8,9]. To do so the 'modified IS', defined as $\Delta_i^{A',A} \times AA'/(A'-A)$, is introduced. When the modified ISs of two transitions (i, j) are plotted against each other (King plot) the points lie on a straight line, with a slope equal to the ratio of the field shift factors, (F_i/F_j), and an intercept equal to $[M_i - (F_i/F_j)M_j]$. In this way, if the mass and field shift factors are known for the transition j, they can also be evaluated for the transition i. King plots are produced here using the IS of the $(5s[3/2]_2–5p[3/2]_2)$ transitions at 760 nm ($j = 760$) measured by Cannon and Janik [22] with an accuracy of about 1 MHz. As an example the King plot for the $5p[5/2]_2$ transition is presented in figure 2, along with a straight line from a weighted linear least-squares fit. The results of King plot analyses are presented in table 3 for four transitions. Since the IS on the $5d[1/2]_1$ transition for the ^{83}Kr isotope is not measured, the King plot does not give significant results, so there are no data reported for this transition. The second and third column contain values from the weighted linear least-squares fit on the King plots. In the last two columns an estimate of F_i and M_i is given, based on values of F_{760} and M_{760} reported in the literature. Both Keim *et al* [25] and Shuessler *et al* [26] have estimated the field and mass shift factors, using a semi-empirical approach and

muonic IS data respectively. Their weighted averages are $F_{760} = -0.605(30)$ GHz fm^{-2} and $M_{760} = 172(17)$ GHz. The highest field shift factor is found for the $6s[3/2]_1$ transition, as expected in an excitation from a p to an s orbital. The large uncertainty in the slope (F_i/F_{760}) hampers physical interpretation of the IS analysis for the $5p[1/2]_0$ and $5p[3/2]_2$ transitions. However, there is an indication, especially for the $5p[5/2]_2$ transition, for a high field shift factor also for transitions from the ground state which do not involve any s electron. This effect is analogous to what was observed in xenon [8, 10], and is ascribed to an increase in the electron density at the nucleus, that results from the removal of a 4p electron from the closed-shell configuration, thereby strongly decreasing the screening of the inner s electrons.

It is noted that a King plot analysis of the data for the ($5s[3/2]_2$–$5p[3/2]_2$) 760 nm transitions versus the data for the $6s[3/2]_1$ transition reported by Trickl *et al* [7] yields a slope of about +2.7. The sign is opposite to that derived from the present data, and it would indicate a decrease in the electron density at the nucleus. This appears to be unrealistic since the excitation is from a p to an s orbital.

3.2. Absolute frequency calibration

Absolute frequency measurements are performed on three transitions, namely $5d[1/2]_1$, $6s[3/2]_1$ and $5p[1/2]_0$, which lie close (i.e. within the scanning range of the ring-dye laser) to a calibrated I_2-line. The main source of systematic uncertainty in the absolute calibration of the transition frequency is the chirp effect in the amplification processes. This effect is estimated to give an uncertainty up to 100 MHz and is sensitive to the specific experimental conditions, especially to the dye used and the wavelength setting of the PDA. The positions of the resonant lines were measured for different pump powers for the PDA. For all the investigated transitions it is found that at high pump power (770 mJ/pulse at 532 nm) the transition frequency is red-shifted compared to low pump power (220 mJ/pulse) measurements. This implies that the laser frequency is shifted upward, and the average shift amongst the three transitions is found to be 109 MHz with a standard deviation of about 40 MHz. Of particular interest is the result obtained for the $5d[1/2]_1$ transition measurement, in which the PDA is running at 578 nm, with the same dye (Rh B) and concentrations as those used by Eikema *et al* [4]. Eikema *et al* [4] developed a technique to actively compensate the chirp effect, and measured a downward shift in the tenth harmonic of the PDA radiation up to 90 MHz when the anti-chirp system was active. We find a shift between high and low PDA pump power measurements of about 66 MHz on the sixth harmonic. If the shift measured by Eikema *et al* [4] is linearly scaled to the sixth harmonic, a value of 54 MHz is found. Hence, the present assessment of the chirp effect is consistent with the findings of [4] and a residual shift of about 10 MHz is left. In the error budget we include, however, a chirp-induced contribution of 30 MHz as a conservative estimate. It has to be noted also that Eikema *et al* [4] performed measurements of the chirp for various wavelengths. Figure 9 of [4] shows that the wavelength dependence of the chirp in the range 577–585 nm is below the 5 MHz level, supporting the estimate of the chirp-induced shift in the present experiment.

Another source of systematic error in the absolute transition frequency calibration originates in the Doppler effect. The crossed beam configuration ensures a low residual Doppler shift, whose value is estimated to be below 20 MHz.

The results of the excited state energy calibrations for the isotope ^{86}Kr performed at low PDA pump power, and the I_2-lines used as references, are presented in table 4. The values of ν_i^{86} reported are the averages over several scans in which the I_2-line and the ^{86}Kr-line are recorded together. The reported uncertainties are the combination of the statistical standard deviation, a residual chirp of 30 MHz, a Doppler uncertainty of 20 MHz, and a small contribution from the

Table 4. Summary of the ^{86}Kr excited state energy calibrations for three transitions; the second column lists the iodine line used for calibration, the third column shows the measured level energy of the state, and in the last column the difference between our results and the values reported by Kaufman and Humphreys [27] are given.

State	I_2 line	ν_i^{86} (cm^{-1})	$(\nu_i^{86} - \nu_{i,KH}^{86})$ (cm^{-1})
$5d[1/2]_1$	P(11)16-1	103 801.8002(12)	−0.0559
$6s[3/2]_1$	P(55)12-2	99 894.0528(14)	−0.0553
$5p[1/2]_0$	R(63)7-4	94 092.8673(13)	−0.0563

uncertainty in the free spectral range of the FPI. In the last column the differences between our result and the values reported by Kaufman and Humphreys [27], $\nu_{i,KH}^{86}$, are shown. Kaufman and Humphreys [27] reported the level energy of several Kr excited states with an internal consistency of 0.0001 cm^{-1}, and an absolute accuracy of 0.15 cm^{-1}. The average value of $(\nu_i^{86} - \nu_{i,KH}^{86})$ is −0.0558 cm^{-1} with a standard deviation of 0.0005 cm^{-1} (15 MHz). The small standard deviation may be taken as a reflection of the high relative precision of our measurements. Also, it is indirect evidence of the small chirp-induced shift since the three krypton lines are measured using different dyes.

Taking into account the possible systematic shift due to both chirp and Doppler effects, a correction of −0.0558(13) cm^{-1} on the energy values by Kaufman and Humphreys [27] is proposed here. This results in a calibration of the excited state energies of Kr to the 0.0013 cm^{-1} level of accuracy. This correction is not entirely consistent with the value −0.0679(61) cm^{-1} suggested by Trickl *et al* [7], who calibrated three VUV-transitions in Kr with a laser system based on a PDA, although both corrections point in the same direction and are of the same order of magnitude. Trickl *et al* [7], however, measured the absolute frequency of the PDA seeding light with respect to Doppler broadened I_2 absorption lines with an uncertainty of 0.001 cm^{-1} (30 MHz), and a +9 MHz shift of their PDA output was assumed without critical discussion. In view of this we claim that our result should be adopted instead, since our standard deviation is more than an order of magnitude smaller.

The new, accurate values of the excited state energies allow for an evaluation of the isotope-dependent ionization energy (E). Yoon and Glab [1] studied krypton Rydberg series excited from the $5p[3/2]_{1,2}$ states, and reported a value of $E = 112\,914.500(14)$ cm^{-1}, where the uncertainty in the initial state energies, corrected according to the suggestion by Trickl *et al* [7], is not considered. When our correction on the energy level values is included instead, then 0.012 cm^{-1} must be added to this value. Moreover, Yoon and Glab [1] performed spectroscopy using natural krypton, in which ^{84}Kr is by far the most abundant isotope, without resolving any isotopic structure. If we assume that the lines they observed are attributed mainly to the ^{84}Kr isotope, then the shift in the $5p[3/2]_{1,2}$ state energies between ^{86}Kr and ^{84}Kr, ∼0.004 cm^{-1} [23], must also be accounted for. In view of these considerations an estimate for the ionization energy of ^{86}Kr, $E^{86} = 112\,914.516(14)$ cm^{-1}, can be given. From this value, ionization energies for the other even isotopes can also be deduced making use of the data reported by Kaufman [23] for the differences of the ionization energies between even isotopes, $E^{n,n-2} \sim 0.008$ cm^{-1}. Finally, it has to be noted that the present estimate of the isotope-dependent ionization energies for krypton is consistent with the isotope-independent value of 112 914.50(2) cm^{-1} adopted by Klar *et al* [28] after a critical discussion on the data reported in the literature.

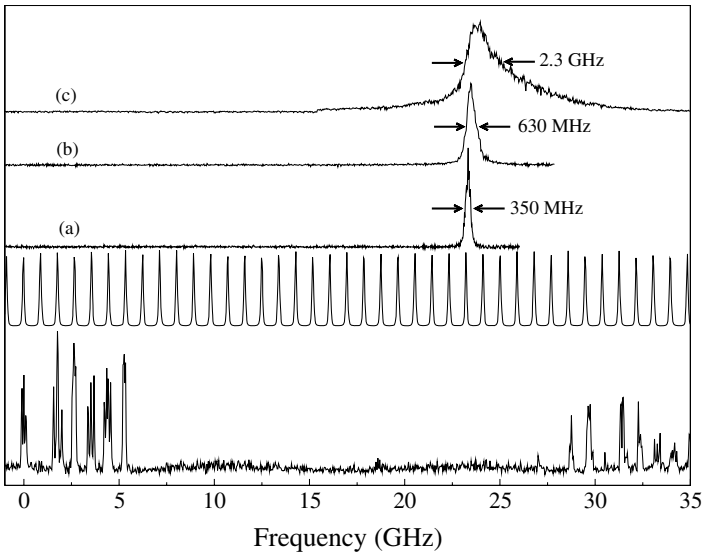

Figure 3. Photoionization spectra of the two-photon $5p[1/2]_0$ transition for ^{84}Kr measured at different power densities: (*a*) $\leqslant$0.2 MW cm^{-2} (*b*) $\sim$260 MW cm^{-2}, (*c*) $\sim$2.6 GW cm^{-2}; the R(63)7-4 I_2 line (on the left) and the etalon markers are also shown; the frequency scale is the actual transition frequency and the zero is set at the '*t*' component of the reference I_2 line.

3.3. Ac Stark effect

The ac Stark effect in an atomic transition arises from the perturbation of the atomic states by a strong time-dependent electro-magnetic field, for example a high-intensity laser pulse. An investigation on the ac Stark effect of the two-photon $5p[1/2]_0$ transition is performed measuring the ^{84}Kr isotope 2UV + 1UV photoionization spectra, and the reference R(63)7-4 I_2 line, for different powers of the UV laser pulses. A $f = 1$ m UV grade fused silica lens is used to increase the UV power density in the interaction region where the beam waist is located. The UV beam diameter at the lens is $\sim$3 mm, and in the interaction region it is $\sim$90 μm (assuming a Gaussian spatial beam profile), resulting in a power density of about 2.6 GW cm^{-2} at 1 mJ/pulse energy. A conservative estimate of the uncertainty in the actual power density of 50% is assumed, related to possible hot spots in the beam. The confocal parameter of the focused beam is about 6 cm, much larger then the diameter of the krypton beam in the interaction region which is of the order of a few millimetres. This justifies the assumption of a plane-wave analysis with nearly constant intensity in the interaction volume. When the focusing lens is not used an upper limit of the power density in the interaction region of about 2 MW cm^{-2} at 1 mJ/pulse energy can be estimated for a collimated UV beam.

In figure 3 typical spectra recorded at different UV pulse energies are shown along with the etalon markers and the I_2 line. The frequency scale is the actual transition frequency, i.e. six times the PDA frequency, relative to the '*t*'-component of the R(63)7-4 I_2 line. Trace (*a*) is recorded without the focusing lens and at low PDA pump power, resulting in a UV energy of 0.1 mJ/pulse ($\leqslant$0.2 MW cm^{-2}); trace (*b*) is obtained under the same conditions as trace (*a*) but using the focusing lens ($\sim$260 MW cm^{-2}); trace (*c*) is the spectrum recorded using the lens and high PDA pump power (1 mJ/pulse UV energy, $\sim$2.6 GW cm^{-2}). The spectrum of trace (*c*) is corrected for a chirp-induced shift of 146 MHz to be consistent with the other traces (see discussion above). The ^{84}Kr line is measured for various UV pulse energies, using

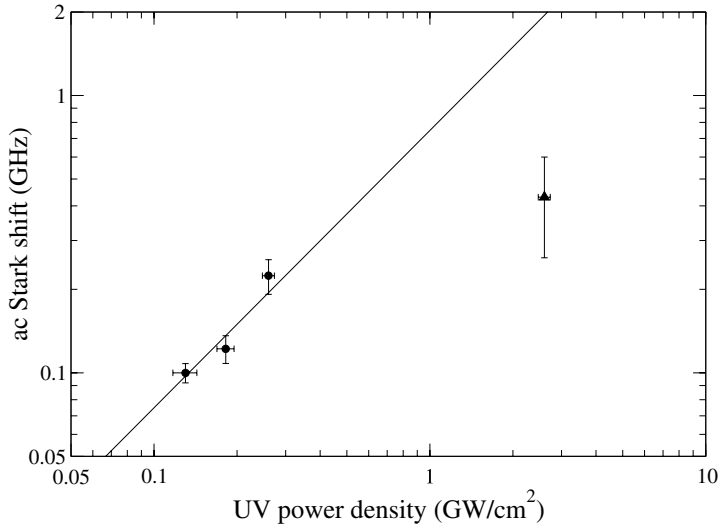

Figure 4. Measured ac Stark shifts on the ($4p^6$–$4p^5 5p[1/2]_0$) two-photon transition in krypton as a function of UV power density; the circles are the low power density data which indicate a linear shift and the straight line is the result of a weighted linear least-squares fit on these data; the triangle is the sub-linear high-intensity shift.

various neutral density filters. The line exhibits a symmetric broadening and a net shift to the blue for power densities up to ∼260 MW cm^{-2}. The full-width at half-maximum of the line measured at ∼260 MW cm^{-2} is ∼630 MHz, compared to 350 MHz measured at low pulse energy without using the focusing lens.

In figure 4 the measured ac Stark shifts are presented in a logarithmic plot. The straight line is the result of a linear least-squares fit on the low UV energy data (circles); the origin is set at the unperturbed transition frequency. The fit yields a slope of 0.75(48) Hz (W cm^{-2})$^{-1}$, where 50% uncertainty on the actual power density is considered, and an intercept of 23.377(44) GHz, which is compatible with the value 23.374(9) GHz obtained without using the lens, i.e. with power density $\leqslant$0.2 MW cm^{-2} (trace (*a*) in figure 3). The high-energy data point (triangle) represents the peak position of trace (*c*) in figure 3, and indicates a sub-linear shift at high UV power density. This is consistent with the result of Camparo and Lambropoulos [29], who performed a Monte Carlo simulation on the ac Stark effect of a two-photon transition assuming a stochastic single-mode light field. At higher laser intensities the resonance shows an asymmetric profile, with a long tail toward higher frequency, i.e. in the direction of the ac Stark shift, and a FWHM of about 2.3 GHz. This is also predicted from ac Stark effect calculations [29–31], and is due to the temporal variation of the actual field intensity during a laser pulse.

3.4. Consequences for narrow-band XUV/VUV generation via two-photon resonance in Kr

The advantageous use of two-photon resonances in Kr and Xe for the resonance-enhanced generation of XUV/VUV radiation has been investigated and implemented in spectroscopic applications by various groups [11–14]. Several orders of magnitude increase in the XUV/VUV yield is obtained if one of the lasers is tuned to resonance in a four-wave mixing scheme, and the $5p[1/2]_0$ resonance has proven to be the most efficient [11]. Particularly for the application of narrow-band radiation in precision spectroscopy, the exact calibration of the two-photon resonances is of importance.

One important application of this scheme has been pursued by the Stoicheff-group [13], determining the dissociation energy of hydrogen. They measured the resonance frequency of the $5p[1/2]_0$ two-photon transition by monitoring resonance-enhanced third-harmonic generation (THG) at 70.9 nm, and reported a value of 94 093.00(4) cm^{-1}, measured with a UV power density of 8×10^8 W cm^{-2}. From our result on the ^{86}Kr transition frequency and the ac Stark shift, we derive a value for this energy of 94 092.89 cm^{-1} at the reported UV power density. A conservative estimate of the uncertainty in this value is 0.02 cm^{-1}, where a small contribution of $\sim$0.005 cm^{-1} from the isotopic composition of natural krypton is also included. Hence, a correction of -0.11 cm^{-1} has to be applied to the calibration of the krypton resonance as well as to the dissociation limit of the hydrogen and deuterium molecule.

Recently also the Merkt-group [14] performed frequency calibration on the same transition by monitoring the resonance-enhanced THG yield. They observed a line at 94 092.91 cm^{-1}, calibrated using the Doppler broadened I_2-reference standard. The UV power density in their experiment can be estimated as 4×10^9 W cm^{-2}, based on the reported pulse energy (50 μJ) and duration (15 ns), focal length of the used lens (16 cm) and assuming a beam diameter at the lens of about 4 mm. We derive a value for the energy of 94 092.90(2) cm^{-1} at this power density, which agrees very well with the calibration based on the THG yield. Also the line-width reported in [14], $\sim$0.12 cm^{-1} (3.6 GHz), is compatible with the ac Stark broadening measured in the present experiment.

Third-harmonic generation and resonant-enhanced multiphoton ionization are processes which may give rise to different calibration results. Phase-matching plays a role in THG and may influence the peak position of the line, as well as does the competition with resonant-enhanced multiphoton ionization. Also, in our crossed beam setup we perform spectroscopic measurements at low densities in the collision-free regime of a skimmed atomic beam, while THG takes place close to the valve of a freely expanding jet where collisions are present. So, a comparison between frequency calibrations based on the two different techniques is not straightforward. Analogous considerations apply also to the ac Stark shift measured by the Stoicheff group, 2.6(1.1) Hz $(W\ cm^{-2})^{-1}$, which is not completely compatible with our finding, although of the same order of magnitude.

An additional feature is of importance in the application of two-photon resonance-enhanced XUV generation. As implicitly demonstrated in the experiment of the Stoicheff group, but not explicitly documented, the resonance also acts as a wavelength-selective element. The XUV-output in [13] allowed for measuring hydrogen resonances at a resolution of 0.25 cm^{-1}, while the bandwidth of the laser at 425 nm (before frequency doubling) was already 0.2 cm^{-1}. Clearly the bandwidth of the XUV radiation is narrower than the convolution of the bandwidth of the incident lasers, when accounting for doubling and two-photon excitation.

A delicate interplay between the wavelength selection, ac Stark effect, isotopic composition, competition between ionization and XUV production, and the collisional effects on the macroscopic nonlinear susceptibility will determine the exact centre frequency and bandwidth of the XUV radiation generated. Future research that can establish the dependences on these parameters and conditions is required.

The application of electromagnetically induced transparency to enhance the efficiency in this wave-mixing scheme is another feature of interest. Dorman *et al* [32] measured high conversion efficiency in a four-wave-mixing scheme via the $(4p^6$–$4p^5 5p[1/2]_0)$ two-photon resonance in Kr, enhanced by electromagnetically induced transparency. The result was obtained by tuning a second laser in resonance with the $(5p[1/2]_0$–$5s[1/2]_1)$ transition at 759 nm, inducing transparency of the medium at the $(4p^6 - 4p^5 5s[1/2]_1)$ transition with a resonant wavelength of 123.6 nm. Dorman *et al* [32] also suggested future investigation of the process with narrow-band UV light.

4. Conclusions

Accurate one-photon VUV and two-photon UV resonantly enhanced photoionization spectroscopy is performed on five transitions from the ground state of krypton. Using a time-of-flight mass spectrometer, spectroscopic information on all stable isotopes is obtained. King plot analyses on the ISs indicate high field-shift factors, even for those transitions in which no s electron is involved. This reveals a large screening effect of the closed-shell p electrons on the inner s electrons, as already shown for xenon.

Absolute frequency calibration is performed for three transitions. A correction of $-0.0558(13)$ cm^{-1} to the excited state energy values reported by Kaufman and Humphreys [27] is suggested. The excited state energies of krypton are determined with an accuracy of about 40 MHz. This result, combined with data reported in the literature, leads to a determination of the ionization energies for all even isotopes.

The ac Stark effect on the two-photon ($4p^6$–$4p^5 5p[1/2]_0$) transition is also investigated. A linear shift of 0.75(48) Hz (W cm^{-2})$^{-1}$ is found for power densities up to 260 MW cm^{-2}. At higher light intensity the line exhibits a sub-linear shift and an asymmetric broadening with a long tail in the direction of the frequency shift.

Finally, consequences of accurate transition frequency calibration for resonance-enhanced narrow-band XUV/VUV generation are discussed. Further investigations are needed to establish the influence of the experimental conditions on the exact central frequency of the XUV/VUV yield, in particular when the generated radiation is used in precision spectroscopy.

References

[1] Yoon S and Glab W L 1994 *J. Phys. B: At. Mol. Opt. Phys.* **27** 4133
[2] Knight R D and Wang L-G 1985 *J. Opt. Soc. Am.* B **2** 1084
[3] Eikema K S E, Ubachs W, Vassen W and Hogervorst W 1993 *Phys. Rev. Lett.* **71** 1690
[4] Eikema K S E, Ubachs W, Vassen W and Hogervorst W 1997 *Phys. Rev.* A **55** 1866
[5] Eikema K S E, Ubachs W and Hogervorst W 1994 *Phys. Rev.* A **49** 803
[6] Velchev I, Hogervorst W and Ubachs W 1999 *J. Phys. B: At. Mol. Opt. Phys.* **32** L511
[7] Trickl T, Vrakking M J J, Cromwell E, Lee Y T and Kung A H 1989 *Phys. Rev.* A **39** 2948
[8] Brandi F, Velchev I, Hogervorst W and Ubachs W 2001 *Phys. Rev.* A **64** 032505
[9] King W H 1984 *Isotope Shifts in Atomic Spectra* (New York: Plenum)
[10] Plimmer M D, Baird P E G, Foot C J, Stacey D N, Swan J B and Woodgate G K 1989 *J. Phys. B: At. Mol. Opt. Phys.* **22** L241
[11] Miyazaki K, Sakai H and Sato T 1989 *Appl. Opt.* **28** 699
[12] Marangos J P, Shen N, Hutchinson M H R and Connerade J P 1990 *J. Opt. Soc. Am.* B **7** 1254
[13] Balakrishnan A, Smith V and Stoicheff B P 1992 *Phys. Rev. Lett.* **68** 2149
Balakrishnan A, Smith V and Stoicheff B P 1994 *Phys. Rev.* A **48** 2460
[14] Hollenstein U, Palm H and Merkt F 2000 *Rev. Sci. Instrum.* **71** 4023
[15] Velchev I, van Dierendonck R, Hogervorst W and Ubachs W 1998 *J. Mol. Spectrosc.* **187** 21
[16] Xu S C, van Dierendonck R, Hogervorst W and Ubachs W 2000 *J. Mol. Spectrosc.* **201** 256
[17] Fee M S, Danzmann K and Chu S 1992 *Phys. Rev.* A **45** 4911
[18] Gangopadhyay S, Melikechi N and Eyler E E 1994 *J. Opt. Soc. Am.* B **11** 231
[19] Melikechi N, Gangopadhyay S and Eyler E E 1994 *J. Opt. Soc. Am.* B **11** 2402
[20] Eyler E E, Yiannopoulou A, Gangopadhyay S and Melikechi N 1997 *Opt. Lett.* **22** 49
[21] Kopfermann H 1958 *Nuclear Moments* (New York: Academic)
[22] Cannon B D and Janik G R 1990 *Phys. Rev.* A **42** 397
[23] Kaufman V 1993 *J. Res. Natl Inst. Stand. Technol.* **98** 717
[24] Aufmuth P, Heiling K and Steudel A 1987 *At. Data Nucl. Data Tables* **37** 455
[25] Keim M, Arnold E, Borchers W, Georg U, Klein A, Neugart R Vermeeren L, Silverans R E and Lievens P 1995 *Nucl. Phys.* A **586** 219

[26] Schuessler H A, Alousi A, Evans R M, Brieger M, Buchinger F and Li Y F 1990 *Phys. Rev. Lett.* **65** 1332
[27] Kaufman V and Humphreys J 1969 *J. Opt. Soc. Am.* **59** 1614
[28] Klar D, Aslam M, Baig M A, Ueda K, Ruf M-W and Hotop H 2001 *J. Phys. B: At. Mol. Opt. Phys.* **34** 1549
[29] Camparo J C and Lambropoulos P P 1992 *J. Opt. Soc. Am.* B **9** 2163
[30] Pindzola M S, Glasser A H and Payne M G 1984 *Phys. Rev.* A **30** 1800
[31] Camparo J C and Lambropoulos P P 1997 *Opt. Commun.* **137** 413
[32] Dorman C, Kucukkara I and Marangos J P 1999 *Phys. Rev.* A **61** 013802